Supplementary Information

Rewritable Wavelength-Selective Hydrogel Actuators Grafted with Fluorophores

Hye Been Koo,[a] Haemin Yeon,[a] Young Bin Yoon,[a] Taek-Jun Lee,[b] Young-Tae Chang,[bc] Jae-Byum Chang*[ad]

[a] *Department of Materials Science and Engineering, Korea Advanced Institute of Science and Technology (KAIST), Daejeon, Republic of Korea*

[b] *Department of Chemistry, Pohang University of Science and Technology, Pohang, Republic of Korea*

[c] *Molecular Imaging Center, Pohang University of Science and Technology, Pohang, Republic of Korea*

[d] *Department of Biological Sciences, Korea Advanced Institute of Science and Technology, Daejeon, Korea*

**Corresponding author: jbchang03@kaist.ac.kr*

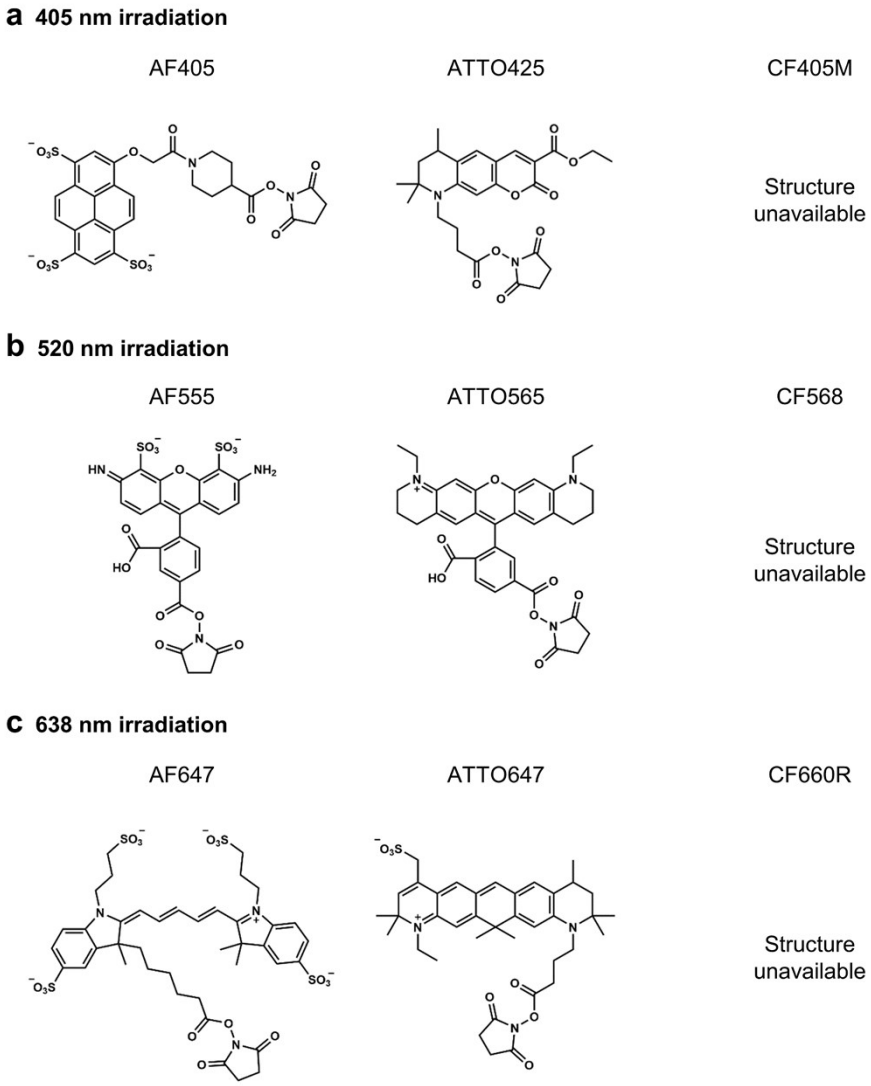

Figure S1. Chemical structures of commercially available fluorophores for a) 405 nm, b) 520 nm, and c) 638 nm laser irradiation.

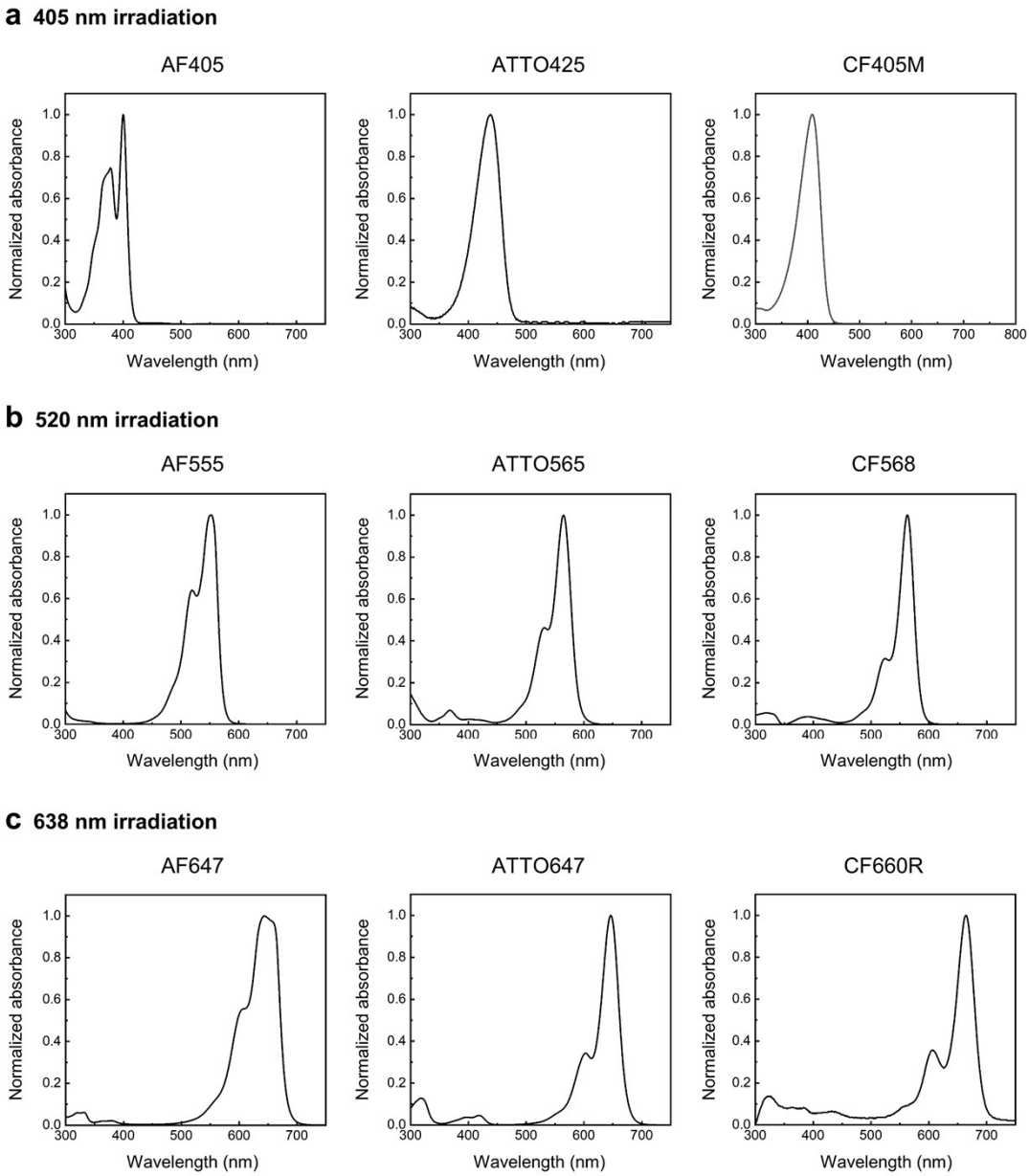

Figure S2. UV-VIS absorption spectra of commercially available fluorophores grafted onto P(NIPAM-*co*-allylamine) hydrogels for a) 405 nm, b) 520 nm, and c) 638 nm laser irradiation.

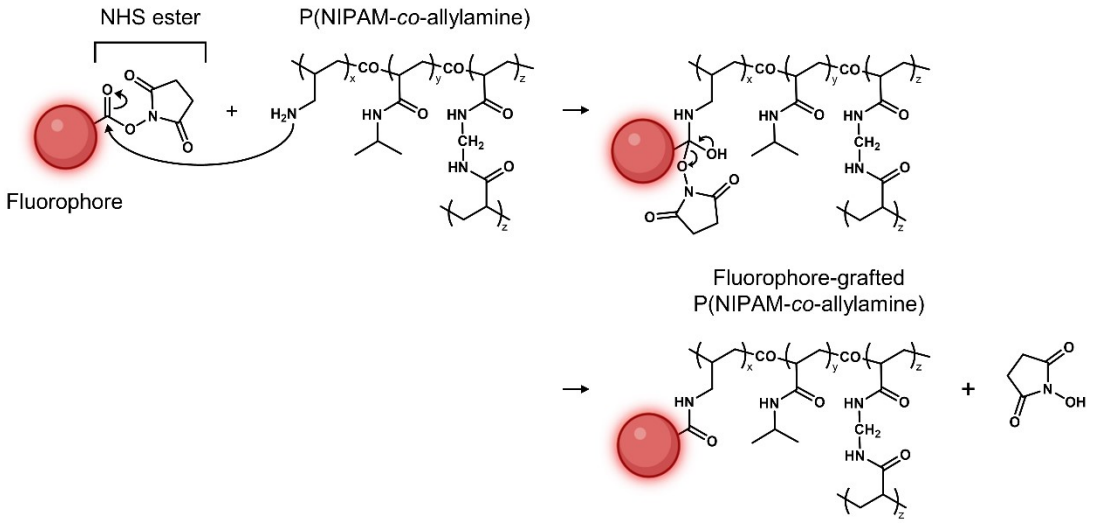

Figure S3. The chemical mechanism of fluorophore grafting in hydrogels for the writing process.

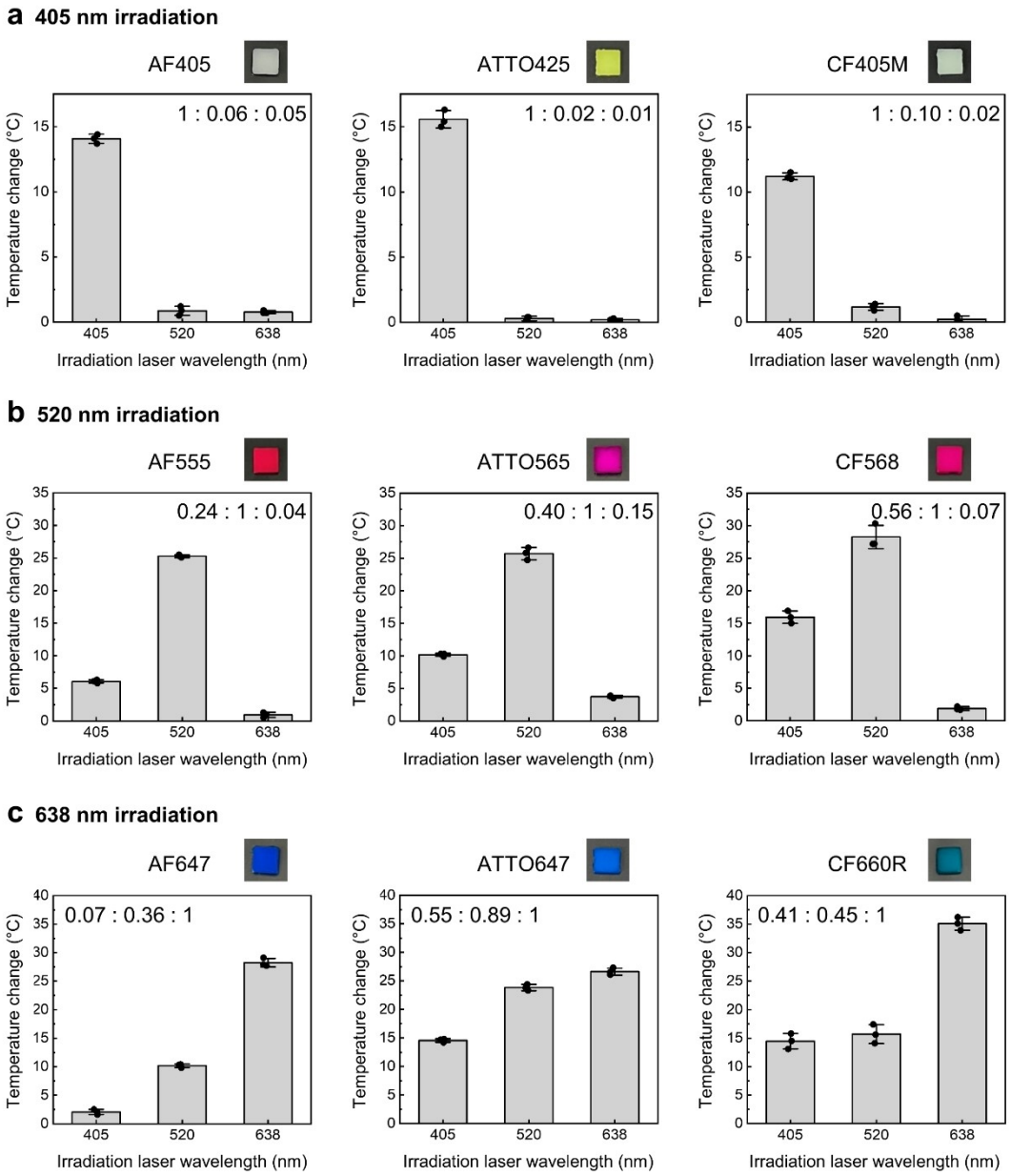

Figure S4. Photothermal effects of commercially available fluorophores under stimulation of lasers with wavelengths of a) 405 nm, b) 520 nm, and c) 638 nm. All data are shown as mean ± s.d. of three independent samples.

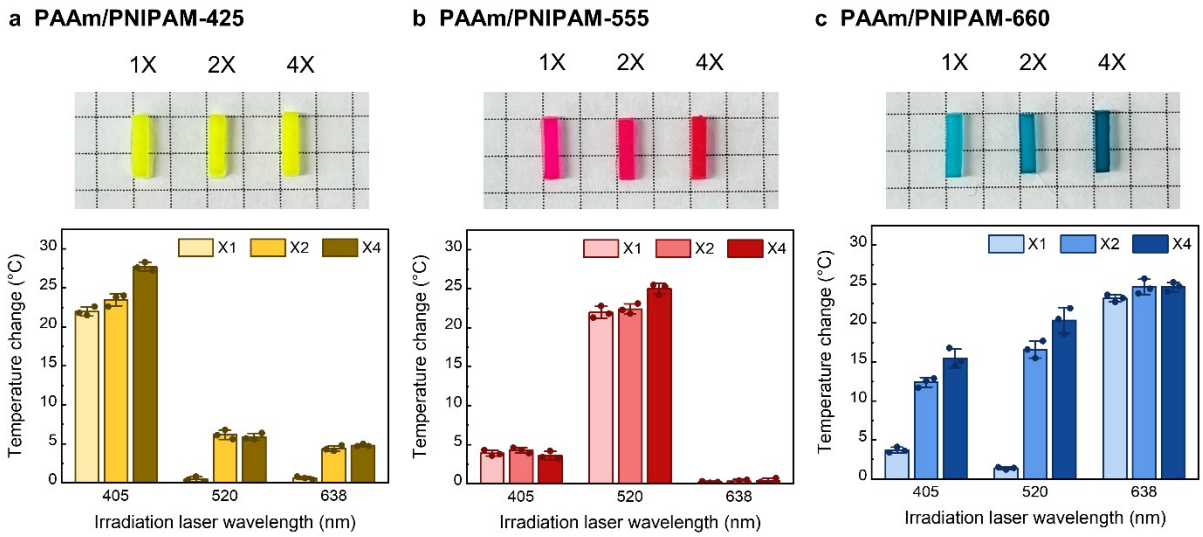

Figure S5. Maximum temperature change of a) PAAm/PNIPAM-425, b) PAAm/PNIPAM-555, and c) PAAm/PNIPAM-660 at optimized fluorophore concentrations of 1X, 2X, and 4X under laser stimulation at wavelengths of 405, 520, and 638 nm. All data are shown as mean ± s.d. of three independent samples.

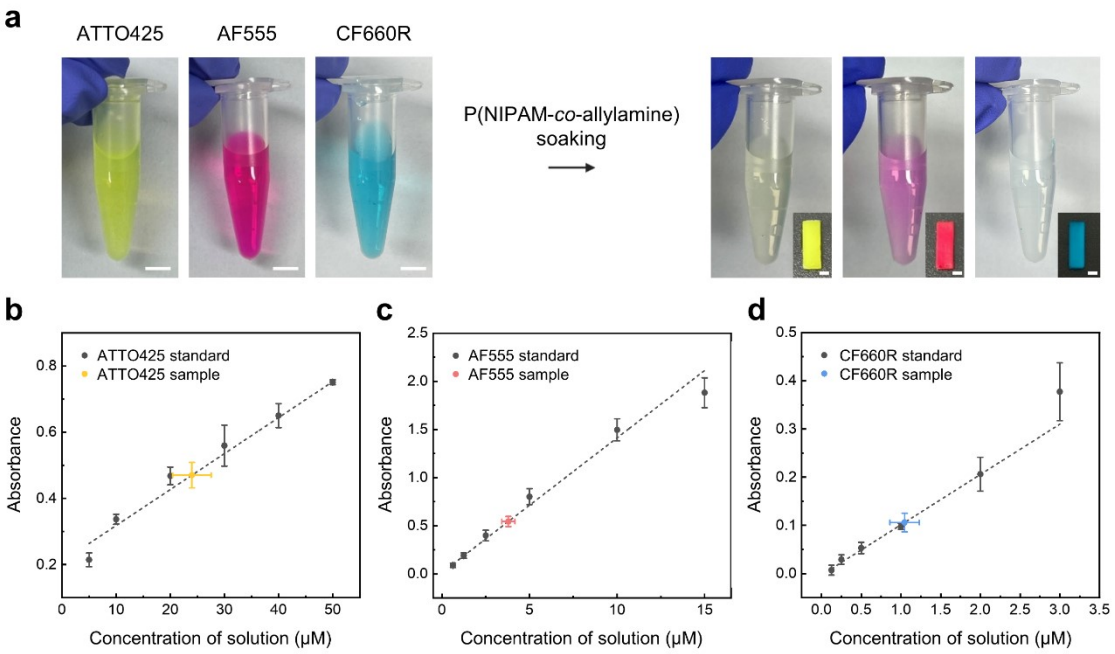

Figure S6. a) Photographs of three fluorophore solutions before and after P(NIPAM-*co*-allylamine) hydrogels. Beer–Lambert calibration curves for b) ATTO425 at 425 nm, c) AF555 at 555 nm, and d) CF660R at 660 nm. All data are shown as mean ± s.d. of three independent samples.

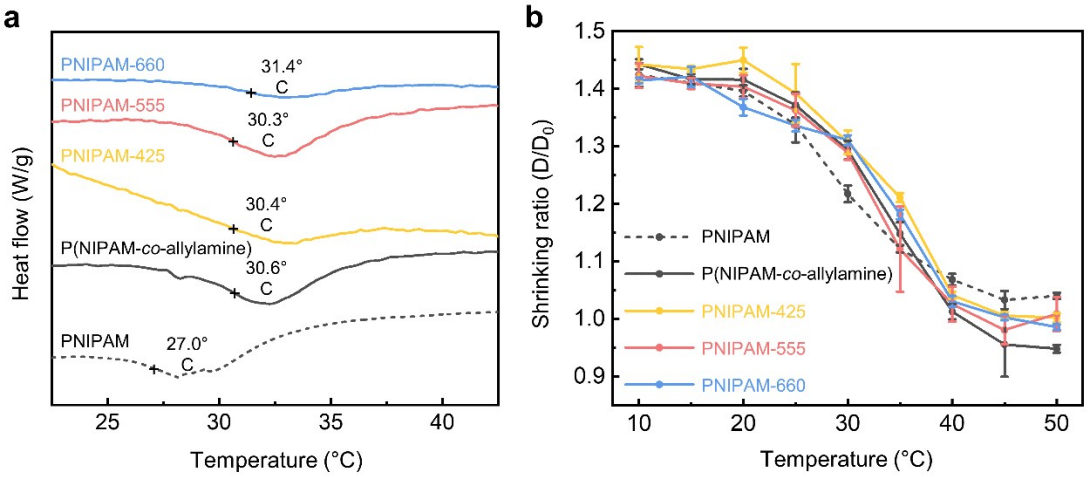

Figure S7. a) DSC curves and b) shrinking ratios as a function of the temperature of PNIPAM, P(NIPAM-*co*-allylamine), and fluorophore-grafted P(NIPAM-*co*-allylamine) hydrogels. Data for shrinking ratios are shown as mean ± s.d. of three independent samples.

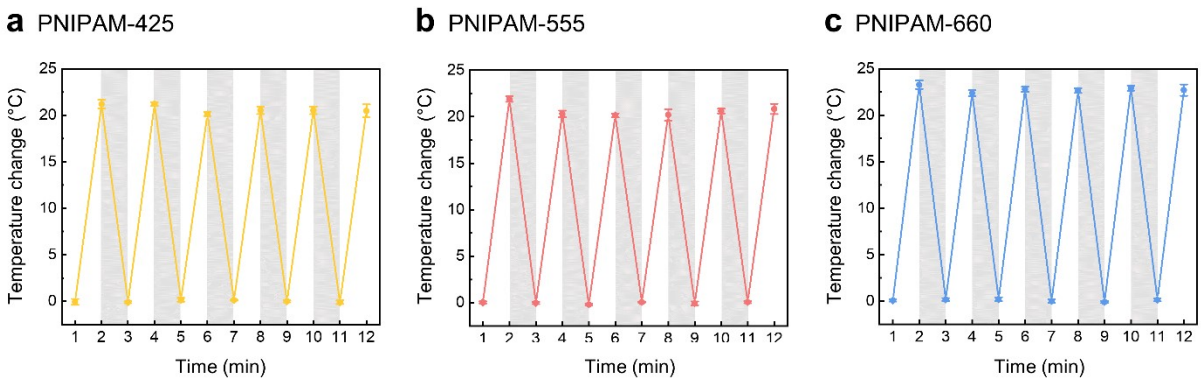

Figure S8. Heating and cooling of fluorophore-grafted hydrogels in multiple irradiation cycles with a) 405 nm, b) 520 nm, and c) 638 nm lights. The 1 min non-irradiation periods are indicated in gray. All data are shown as mean ± s.d. of three independent samples.

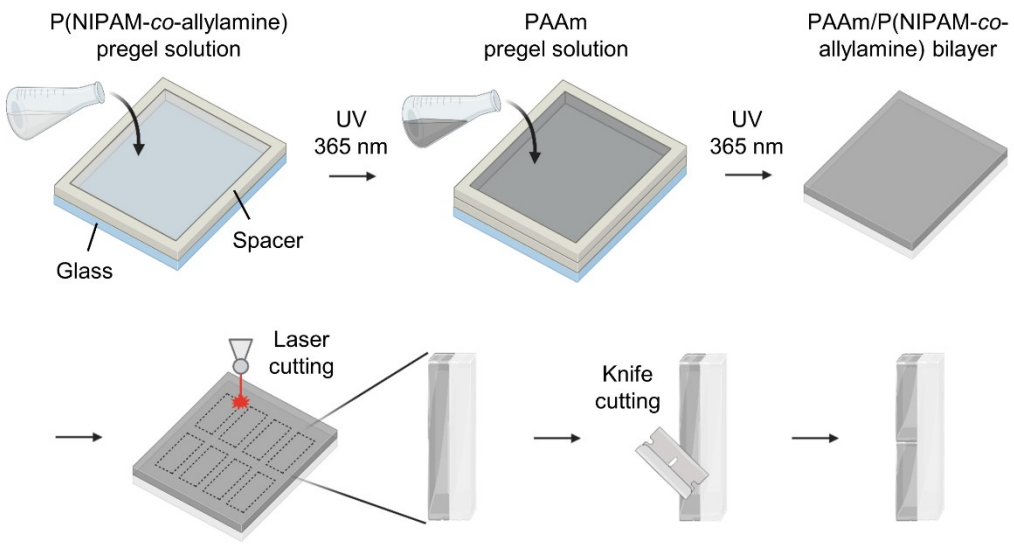

Figure S9. Schematic illustration of the fabrication process of PAAm/P(NIPAM-*co*-allylamine) hydrogel bilayers.

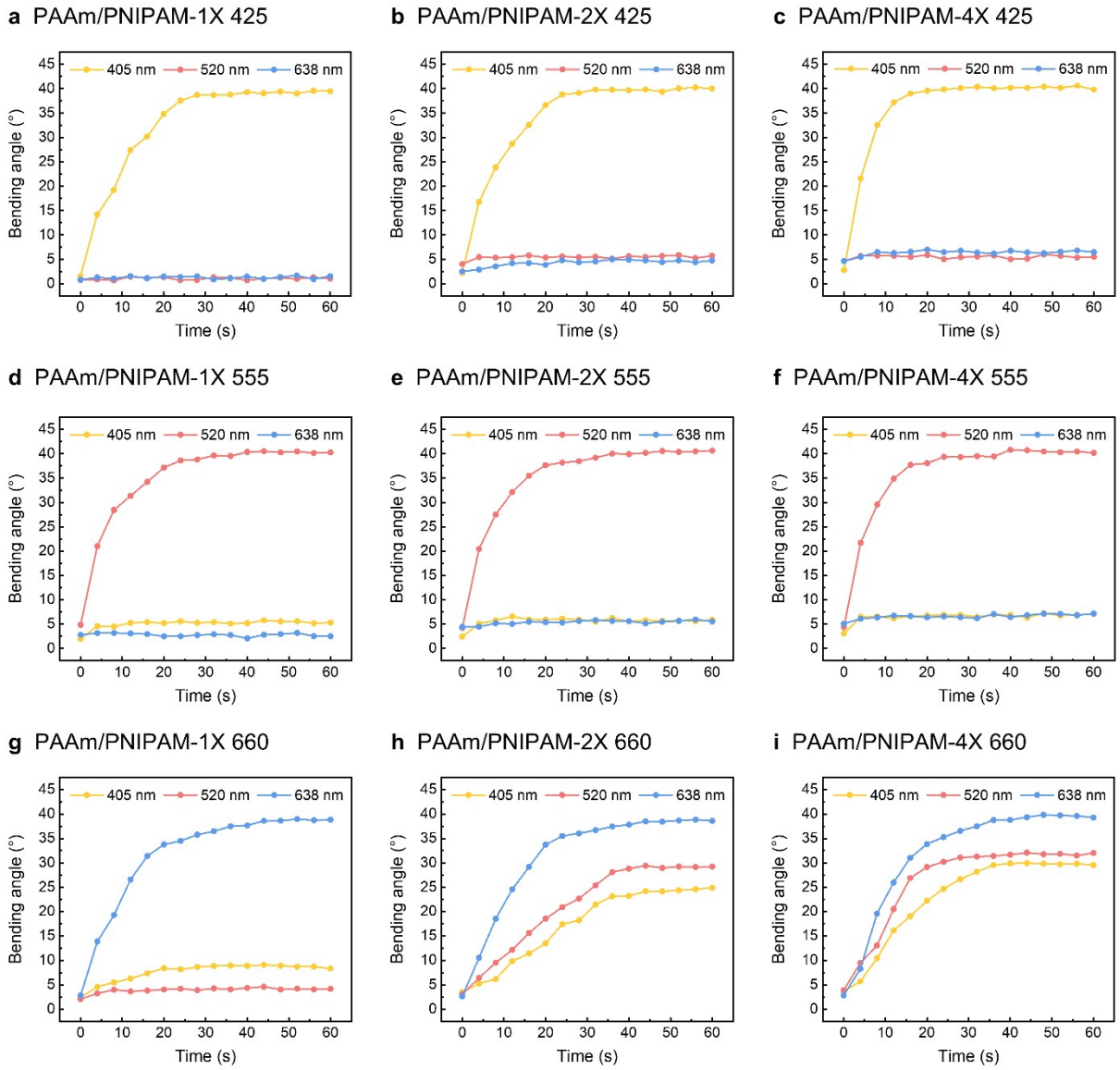

Figure S10. Bending angle responses of PAAm/PNIPAM hydrogels with varying fluorophore concentrations (1X, 2X, and 4X) under laser irradiation at 405 nm, 520 nm, and 638 nm. a–c) PAAm/PNIPAM-425 with ATTO425 at 1X, 2X, and 4X concentrations. d–f) PAAm/PNIPAM-555 with AF555 at 1X, 2X, and 4X concentrations. g–i) PAAm/PNIPAM-660 with CF660R at 1X, 2X, and 4X concentrations. All data presented were obtained from a single sample for each condition.

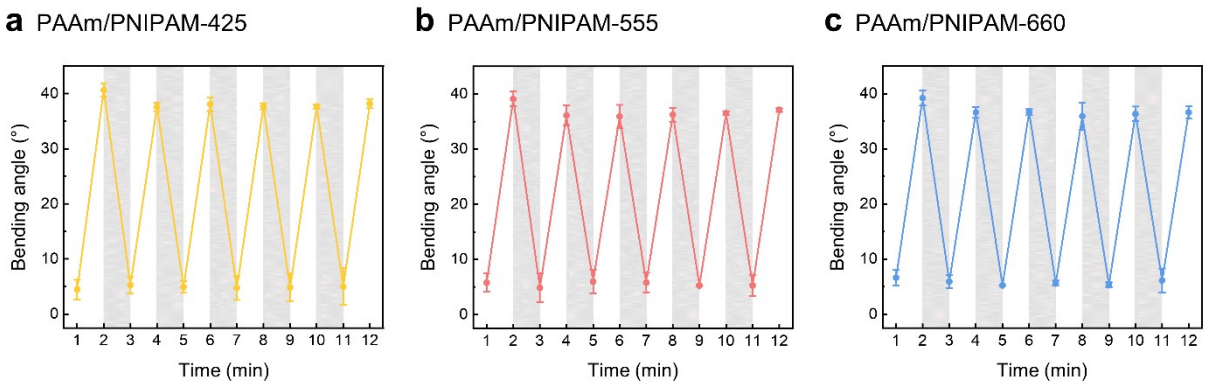

Figure S11. Bending and recovery of fluorophore-grafted hydrogel bilayers in multiple actuation cycles upon irradiation with a) 405 nm, b) 520 nm, and c) 638 nm lights. The 1 min non-irradiation periods are indicated in gray. All data are shown as mean ± s.d. of three independent samples.

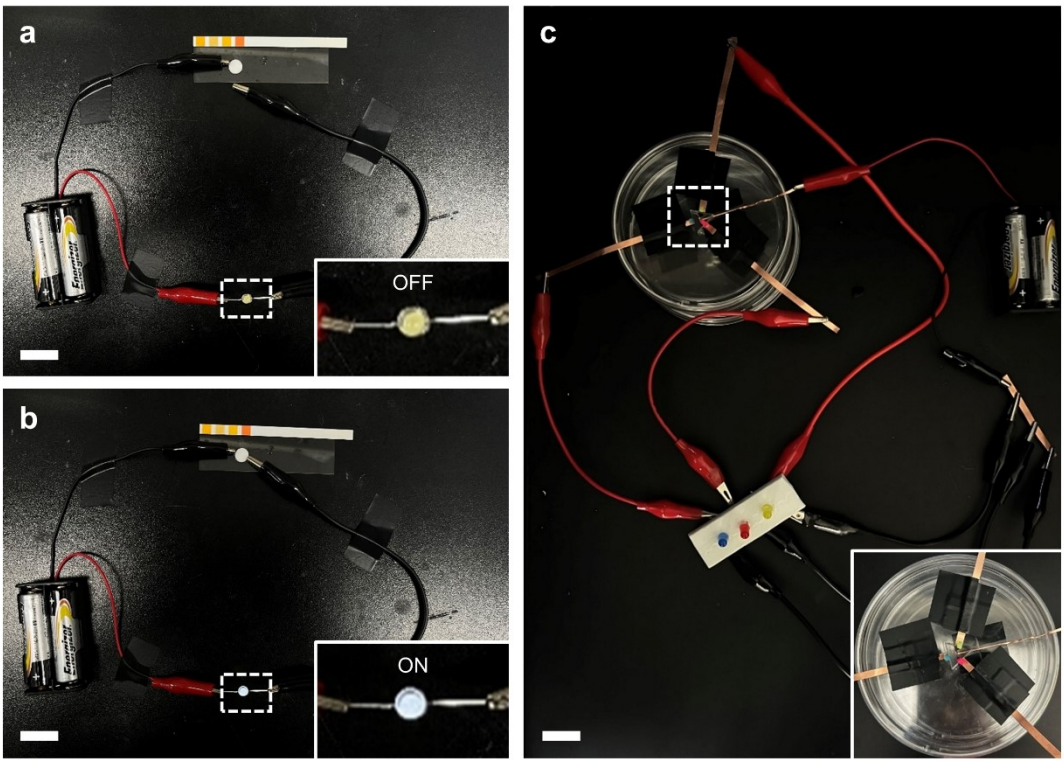

Figure S12. a) Non-ionic conductivity for the P(NIPAM-*co*-allylamine) hydrogel without lighting an LED. b) Ionic conductivity for the P(NIPAM-*co*-allylamine) hydrogels after soaking in 0.1M KH_2PO_4 at pH 7.4 with lighting an LED. c) Photograph of a circuit for a demonstration of fluorophore-grafted hydrogel bilayers as wavelength-selective switches.

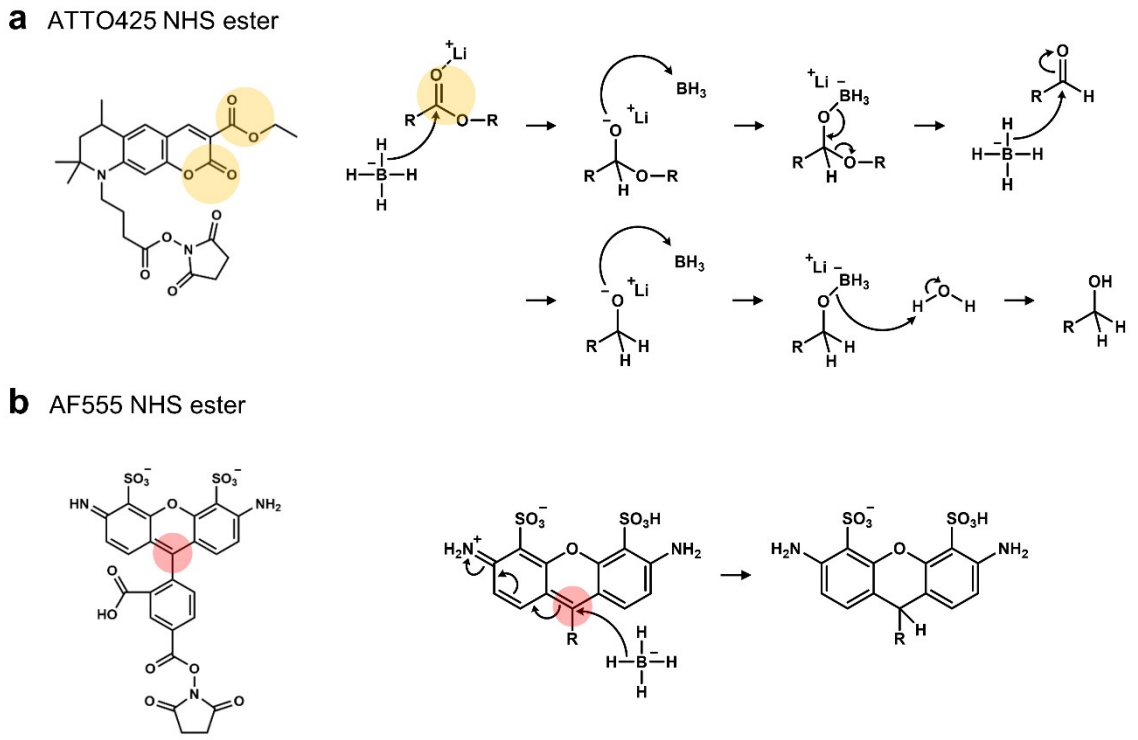

Figure S13. The chemical mechanisms of a) the reduction of the ester group in ATTO425 and b) the hydrogen transfer reaction in AF555 upon $LiBH_4$ treatment.

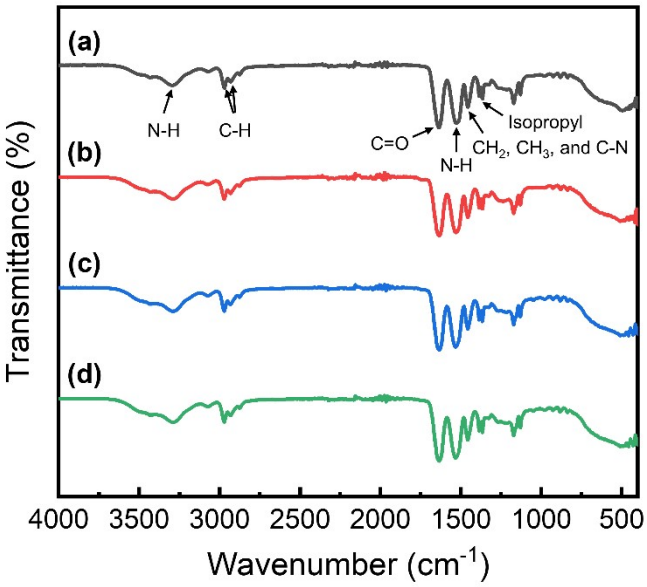

Figure S14. The ATR-FTIR spectra of a) PNIPAM-425 before bleaching, b) PNIPAM-425 after bleaching, c) PNIPAM-555 before bleaching, and d) PNIPAM-555 after bleaching.

The characteristic vibration band at 1635 cm^{-1} indicates N–H groups and C=O stretching in the NIPAM units of the copolymer. The peak around 1455 cm^{-1} corresponds to CH_3 antisymmetric bending, CH_2 scissoring, and C–N stretching of the amide groups, while the 1365 cm^{-1} peak is attributed to the symmetric bending of the isopropyl groups from PNIPAM. Peaks at 2972 cm^{-1} and 2935 cm^{-1} indicate the C–H stretching of alkyl carbons. The 3292 cm^{-1} peak represents the N–H bending of amine groups, and the strong band at 1531 cm^{-1} corresponds to the N–H stretching of allylamine groups.

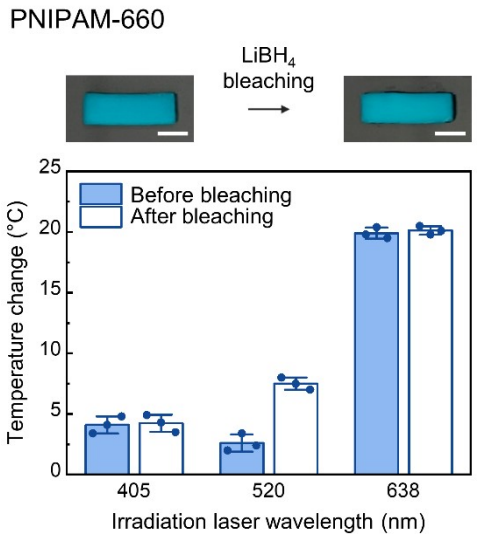

Figure S15. Photograph and the change in the photothermal effect of PNIPAM-660 hydrogels under 405 nm, 520 nm, and 638 nm light illumination before and after chemical bleaching. Data are shown as mean ± s.d. of three independent samples.

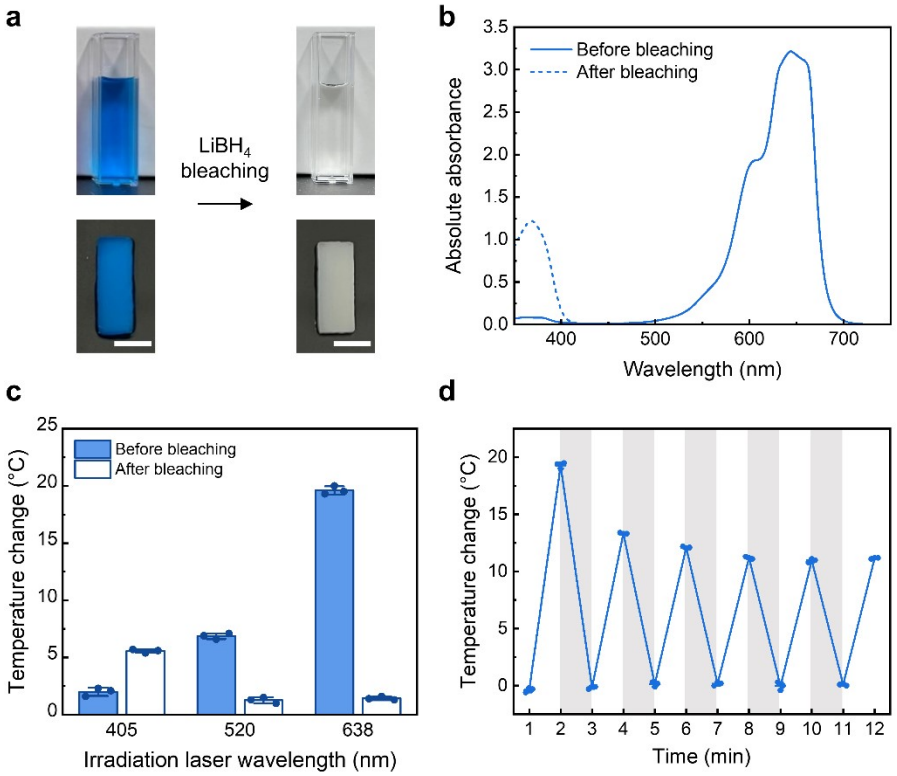

Figure S16. a) Photographs of the fluorophore solution and PNIPAM-647 hydrogel with AF647 before and after bleaching. b) UV–VIS absorption spectra of PNIPAM-647 before and after bleaching. c) Photothermal effects of PNIPAM-647 under the stimulation of lasers with wavelengths of 405 nm, 520 nm, and 638 nm. d) Heating and cooling of PNIPAM-647 in multiple irradiation cycles at 638 nm. All data are presented as mean ± s.d. of three independent samples.

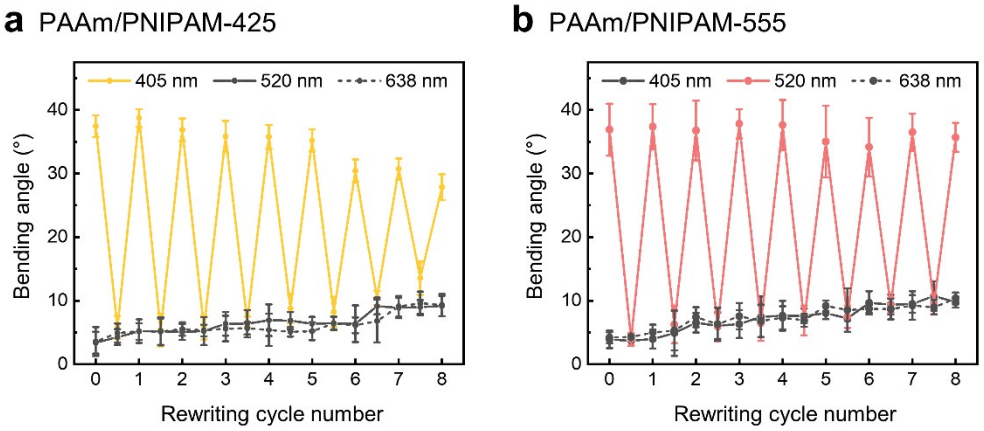

Figure S17. For sequential multiple rewriting processes, the variations in bending angles of a) PAAm/PNIPAM-425 and b) PAAm/PNIPAM-555 bilayers under the stimulation of lasers with wavelengths of 405, 520, and 638 nm. All data are shown as mean ± s.d. of three independent samples.

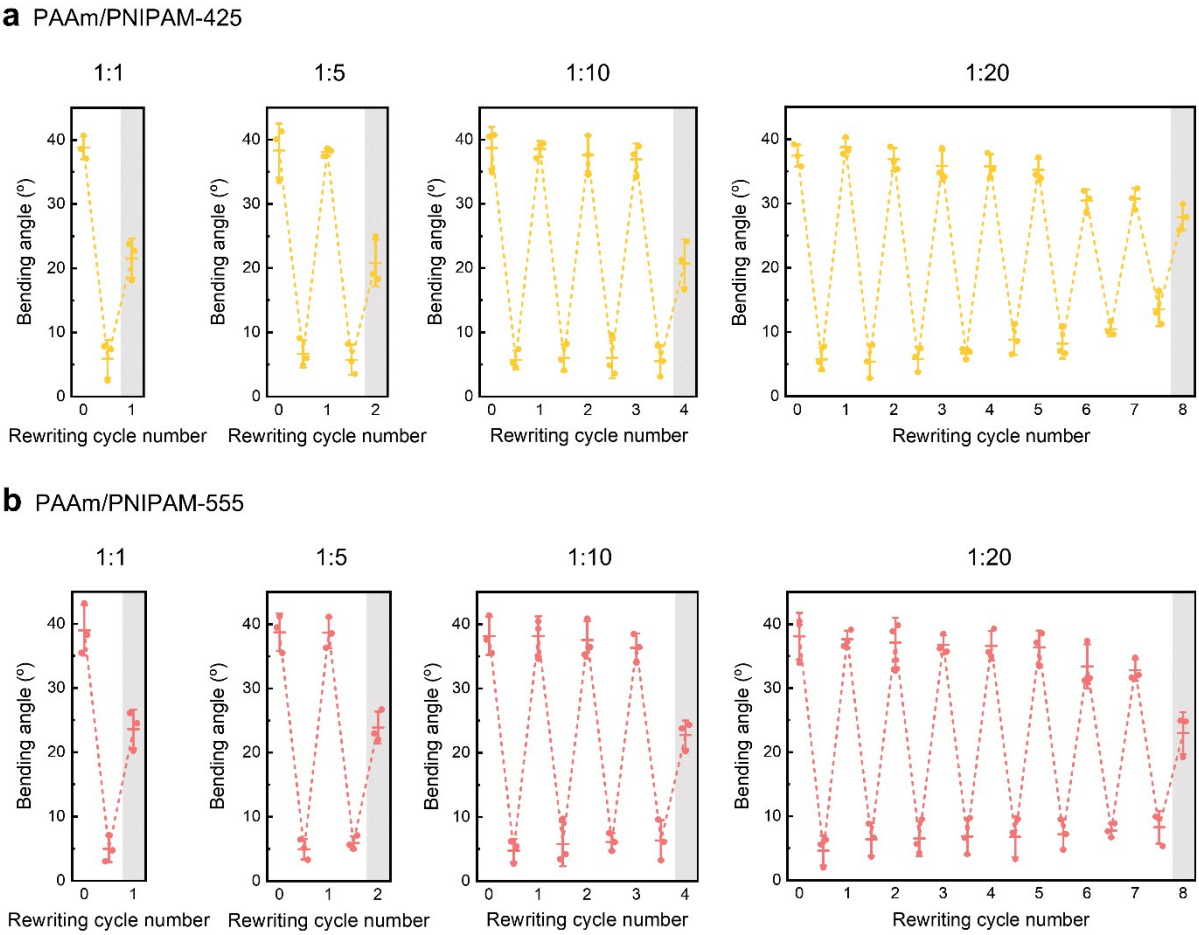

Figure S18. The rewritable cycle numbers of a) PAAm/PNIPAM-425 and b) PAAm/PNIPAM-555 bilayers with different molar ratios of fluorophores to allylamine. All data are presented as mean ± s.d. of three independent samples.

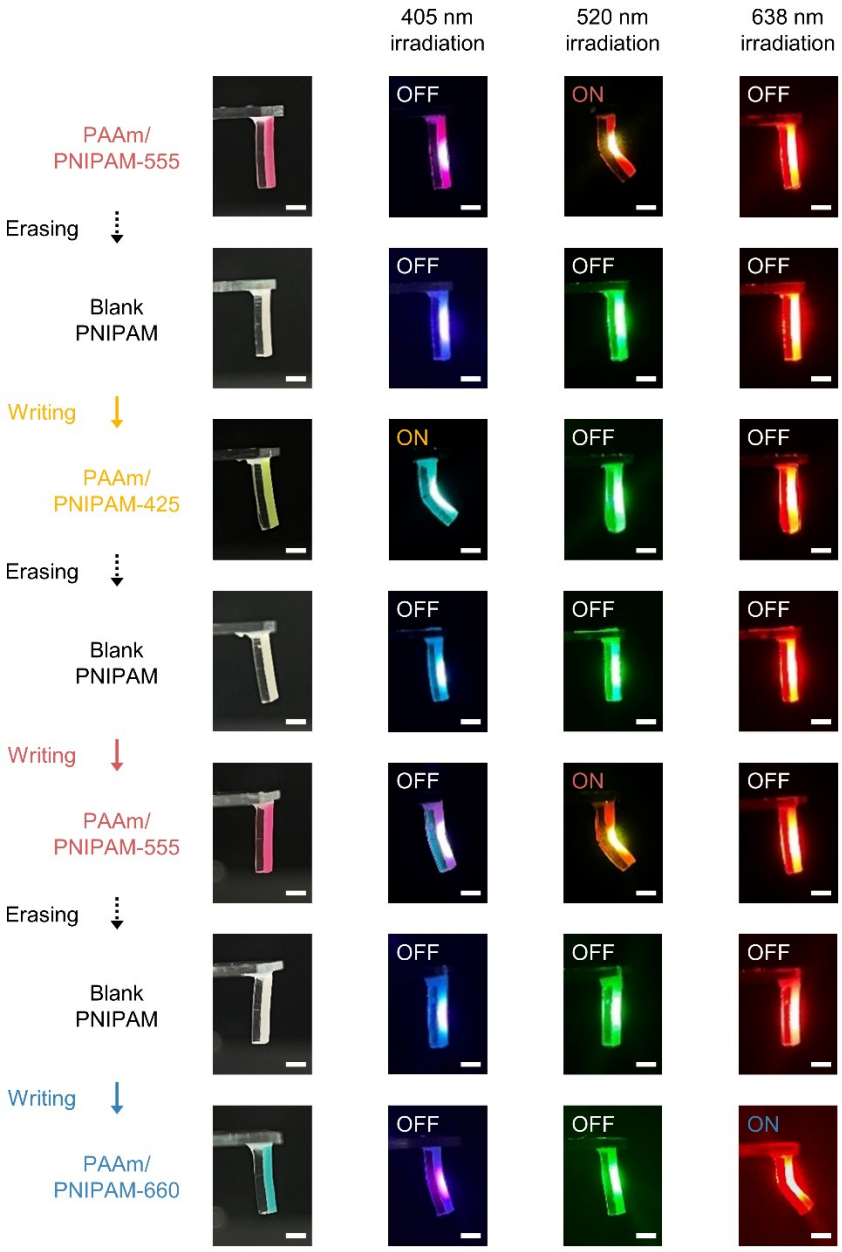

Figure S19. For sequential multiple rewriting processes, photographs of a single bilayer under the stimulation of lasers with wavelengths of 405, 520, and 638 nm in each rewriting.

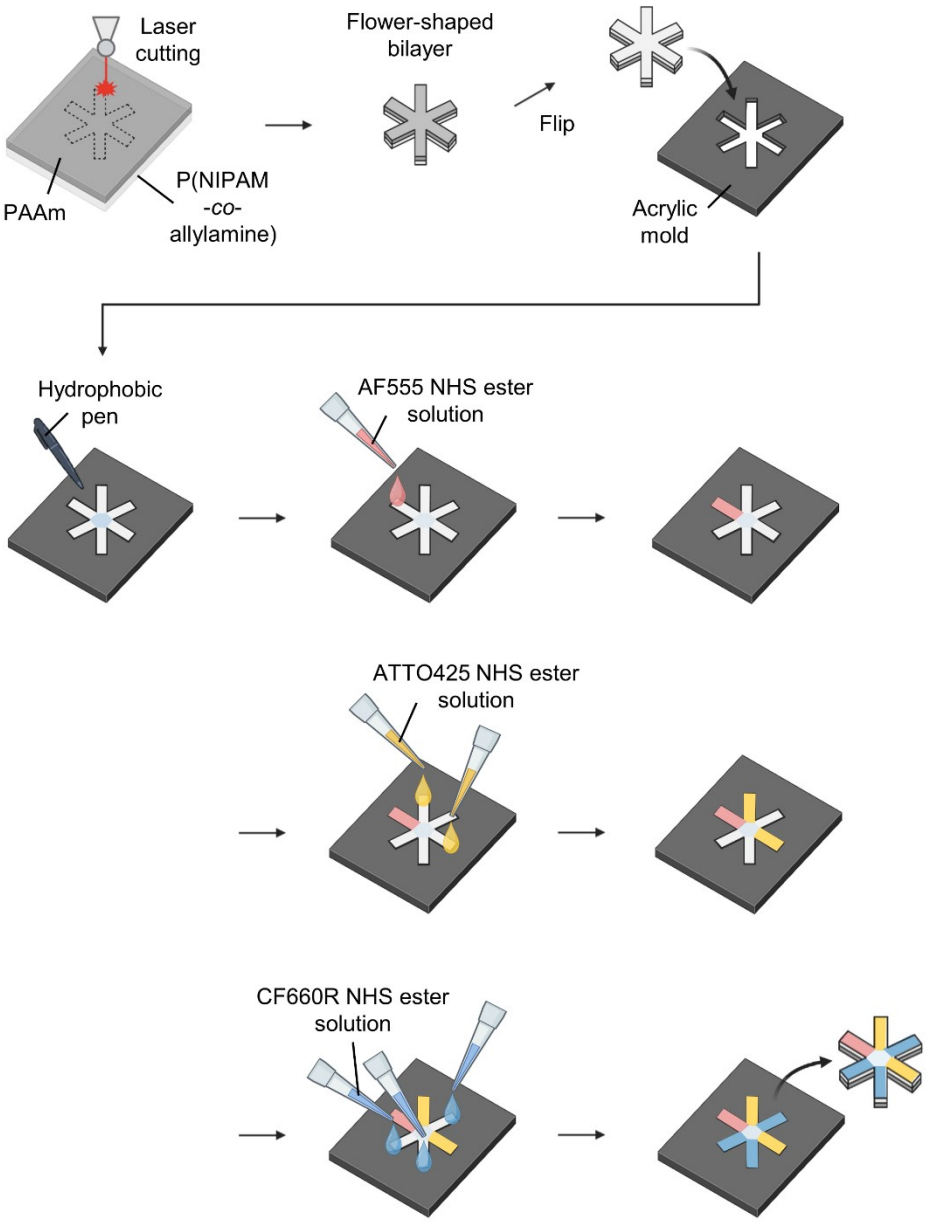

Figure S20. Schematic illustration of the fabrication process for flower-shaped hydrogel actuators grafted with three fluorophores.

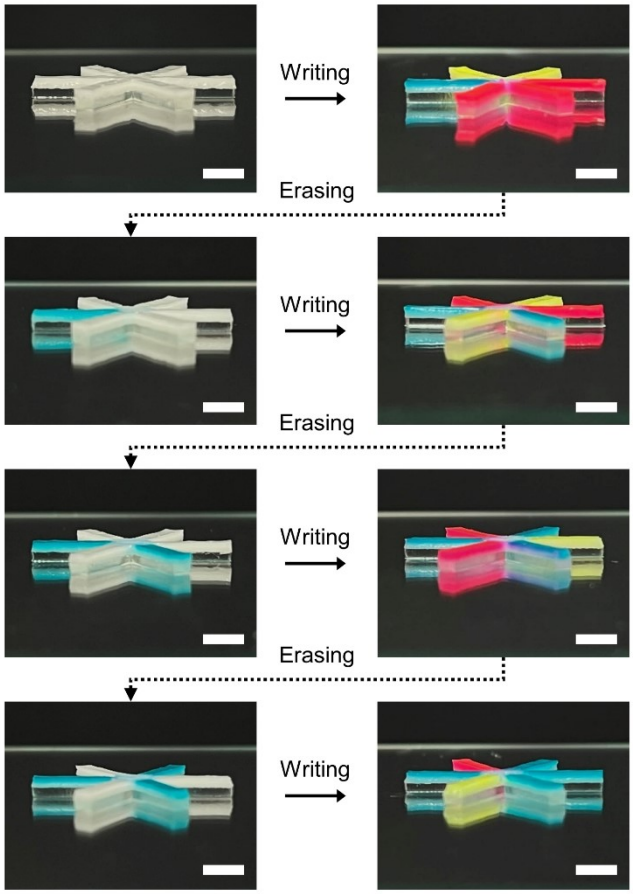

Figure S21. For sequential multiple rewriting processes, photographs of a single flower-shaped hydrogel actuator in each writing and erasing process.

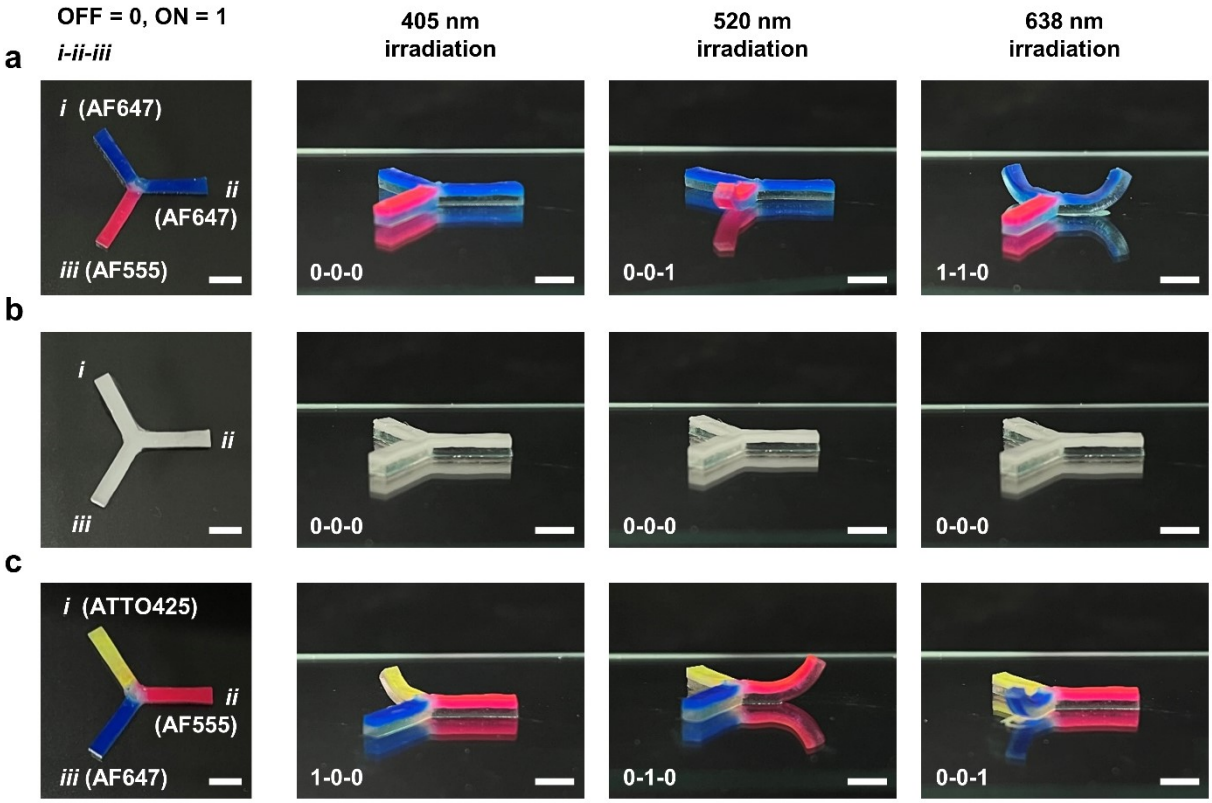

Figure S22. Three rewritable wavelength-selective hydrogel actuators in a three-petal flower shape grafted with ATTO425, AF555, and AF647. Photographs of wavelength-selective photoactuation from a single hydrogel actuator after a) writing, b) erasing, and c) rewriting via sequential rewriting processes. The three leaves of the resulting flower-shaped hydrogel actuator were designated *i, ii,* and *iii* in clockwise order, with the initial unbent state defined as 0 and the bent state after laser irradiation defined as 1.

Table S1. Multiple configurations of a single flower-shaped hydrogel actuator via iterative rewriting processes. Note that ON denotes the bending deformation, and OFF denotes the initial state.

Number of writing	Irradiation laser wavelength	*i*	*ii*	*iii*	*iv*	*v*	*vi*
1st	405 nm	OFF	ON	ON	OFF	OFF	OFF
1st	520 nm	OFF	OFF	OFF	ON	ON	ON
1st	638 nm	ON	OFF	OFF	OFF	OFF	OFF
2nd	405 nm	OFF	OFF	ON	OFF	OFF	ON
2nd	520 nm	OFF	ON	OFF	ON	OFF	OFF
2nd	638 nm	ON	OFF	OFF	OFF	ON	OFF
3rd	405 nm	OFF	OFF	OFF	ON	OFF	OFF
3rd	520 nm	OFF	ON	OFF	OFF	OFF	ON
3rd	638 nm	ON	OFF	ON	OFF	ON	OFF
4th	405 nm	OFF	OFF	OFF	OFF	OFF	ON
4th	520 nm	OFF	ON	OFF	OFF	OFF	OFF
4th	638 nm	ON	OFF	ON	ON	ON	OFF

Movie S1. Bending and recovery of the PAAm/PNIPAM-425 bilayer under 405, 520, and 638 nm irradiation.

Movie S2. Bending and recovery of the PAAm/PNIPAM-555 bilayer under 405, 520, and 638 nm irradiation.

Movie S3. Bending and recovery of the PAAm/PNIPAM-660 bilayer under 405, 520, and 638 nm irradiation.